Mechatronics, Electrical Power, and Vehicular Technology 03 (2012) 87-94

Mechatronics, Electrical Power, and Vehicular Technology

e-ISSN: 2088-6985
p-ISSN: 2087-3379
Accreditation Number: 432/Akred-LIPI/P2MI-LIPI/04/2012

www.mevjournal.com

ANALYTICAL AND NUMERICAL DEFLECTION STUDY ON THE STRUCTURE OF 10 KW LOW SPEED PERMANENT MAGNET GENERATOR

KAJIAN DEFLEKSI ANALITIS DAN NUMERIK PADA STRUKTUR GENERATOR MAGNET PERMANEN KECEPATAN RENDAH KAPASITAS 10 KW

Hilman S. Alam [a,*], Pudji Irasari [b], Dyah Kusuma Dewi [c]

[a] Technical Implementation Unit for Instrumentation Development, Indonesian Institute of Sciences, Jl. Sangkuriang Komplek LIPI Gedung 30 Bandung, 40135, Indonesia

[b] Research Center for Electrical Power and Mechatronics, Indonesian Institute of Sciences, Jl. Sangkuriang Komplek LIPI Gedung 20 Lantai 2 Bandung, 40135, Indonesia

[c] Directorate of Technology for Manufacturing Industry, Agency for Assessment and Application of Technology, Gedung Teknologi 2 Puspitek Serpong, Tangerang, Indonesia

Received 23 October 2012; Received in revised form 01 December 2012; Accepted 03 December 2012
Published online 18 December 2012

Abstract

Analytical and numerical studies of the deflection in the structure of 10 kW low speed permanent magnet generator (PMG) have been discussed in this paper. This study is intended to prevent failure of the structure when the prototype is made. Numerical analysis was performed with the finite-element method (FEM). Flux density, weight and temperature of the components are the required input parameters. Deflection observed were the movements of the two main rotor components, namely the rim and shaft, where the maximum deflection allowed at the air gap between rotor and stator should be between 10% to 20% of the air gap clearance or 0.1000 mm to 0.2000 mm. Base on the analysis, total deflection of the analytic calculation was 0.0553 mm, and numerical simulation was 0.0314 mm. Both values were in the acceptable level because it was still below the maximum allowed deflection. These results indicate that the structure of a permanent magnet generator (rim and shaft) can be used safely.

Key words: permanent magnet generator, finite element, air gap, deflection.

Abstrak

Studi secara analitis dan numerik mengenai defleksi pada struktur generator magnet permanen (GMP) kecepatan rendah kapasitas 10 kW telah dibahas dalam makalah ini. Studi ini dimaksudkan untuk mencegah kegagalan struktur saat prototipe sudah dibuat. Analisis numerik dilakukan dengan metode elemen hingga (MEH). Kerapatan fluks, berat dan suhu komponen merupakan parameter-parameter masukan. Defleksi yang diamati adalah gerakan dua komponen utama rotor yaitu rim dan poros, di sini defleksi maksimum yang diizinkan pada celah udara antara rotor dan stator harus berkisar antara 10% sampai 20% dari clearance celah udara atau 0,1000 mm sampai 0,2000 mm. Berdasarkan hasil analisis, defleksi total hasil perhitungan analitis adalah 0,0553 mm sedangkan simulasi numerik adalah 0,0314 mm. Kedua nilai tersebut memenuhi persyaratan karena masih di bawah defleksi maksimum yang diizinkan. Hasil tersebut menunjukkan bahwa struktur generator magnet permanen (rim dan poros) dapat digunakan secara aman.

Kata kunci: generator magnet permanen, elemen hingga, celah udara, defleksi.

I. INTRODUCTION

In general, the constructions of low-speed high torque permanent magnet generators (PMG) tend to have large dimension, heavy and expensive. The major costs are caused by materials, installation and transportation. The construction of the radial flux PMG is dominated by the weight of inactive components that is equal to 2/3 of the total weight, while the rest is that of the active components (iron, copper, and permanent magnet) [1]. They serve as a support to keep the clearance at the air gap and to hold

* Corresponding Author. Tel: +62-81394297528
E-mail: alam_hilman@yahoo.com

doi: 10.14203/j.mev.2012.v3.87-94

the active components to stay in place when subjected to normal force, shear force and thermal effects.

Reducing the weight of generator is an issue of interest to designers and manufacturers. This is because the inactive structure of direct drive generator is directly connected to the prime mover and its weight can reach 80% of the total [1]. It is needed to counteract the magnetic attractive force between the stationary and moving parts and it is influenced by the type and nature of the material used. Tensile stress is generated by normal/Maxwell force that could reach ten times the shear stress. Distance or clearance between the rotor and the stator must be maintained to avoid damage to the PMG [2,3]. Research to find potential solutions in terms of geometry, materials and sources of excitation becomes an important issue to increase market competition, reducing prices and weights of components so that the efficiency and reliability of PMG can be improved [3].

Design of the generator in this study is focused on the rotor shaft that serves as a support structure of active components. One important step in the design is stress analysis on the structure, which will find the number of iterations to meet allowable rotor deflection before manufacturing of prototypes. Stress analysis based on an analytical approach then is validated by numerical methods or also called finite element method (FEM).

The method has been applied to the analysis of electromagnetic in some earlier studies [1-10]. Several advantages over other numerical methods are: it gives detailed and exact analysis and computation [5][9]; it provides an efficient solution [6]; it is able to analyze various types of electrical machines, including permanent magnet parametric geometry, post processing and visualization of results [10].

II. METHODOLOGY

Clearance on generator is generally calculated as 1/1000 of the air gap diameter [1]. For 10 kW of capacity, the PMG with air gap radius, r_g = 168.5 mm will need 0.1685 mm of clearance. The allowed deflection of the rotor ranges from 10-20% [1]. Figure 1 shows a cross-section of radial flux PMG. Air gap between the stator and rotor is designed to be 1 mm, greater than it should be (0.1685 mm) due to manufacturing consideration, then the maximum deflection of the air gap clearance to be ranged between 0.100 mm to 0.200 mm.

The parameters, which affect the deflection of the structure consist of flux density $\hat{B}$, mass of

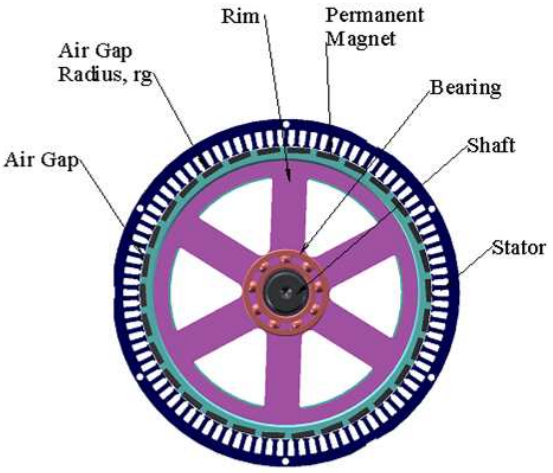

Figure 1. Cross section of the radial flux PMG.

the component M and the temperature difference ΔT. They are used as inputs to calculate the normal stress, weight of the components and the thermal expansion of the material. Design is analytically calculated and the results are validated using FEM. The allowable maximum deflection is used as a consideration in the design iteration. Input data is obtained from the calculation using the FEM. Figure 2 shows the method used in designing the structure of PMG to target 10-20% total deflection of the air gap clearance.

A. The Existence of Forces on PMG

The distance between the rotor and stator in the PMG, is one of the most critical factors in the design considerations. Besides affected by weight of the part itself, deflection is also influenced by the air gap flux density. If it increases, the normal

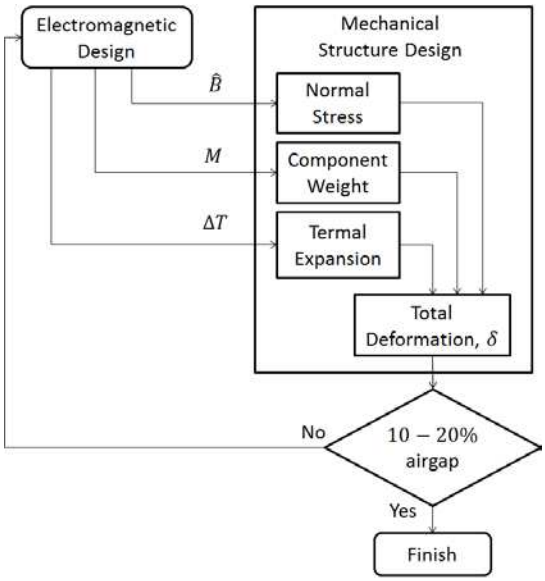

Figure 2. Design methodology of the PMG.

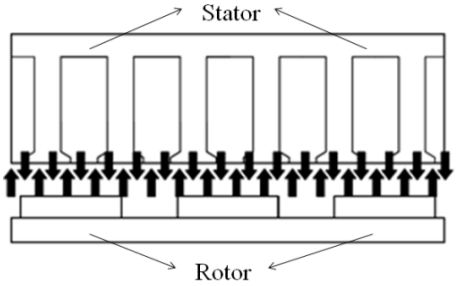

Figure 3. Cross-section of the PMG with normal voltage along the air gap.

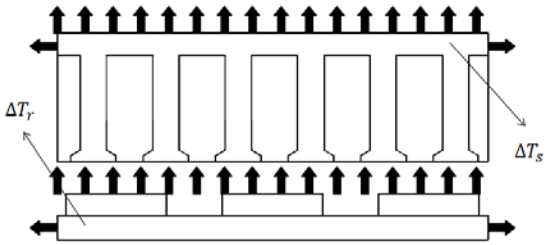

Figure 5. Expansion due to temperature rise in the stator ΔT_s and rotor ΔT_r.

stress and deflection in the rotor will rise higher. In addition subjected to normal stresses, PMG is subjected to a shear stress as well. Shear stress is one of the important factors in the design as it relates to the torque to be generated [1].

Normal stresses on PMG occur in the normal direction or lead directly to the air gap, see Figure 3.

Normal stresses on the stator and rotor move in and out radially and are larger than the shear stress. When the flux density, $\hat{B}$ in the air gap rises (during operation: $\hat{B}$ >0.8T), the normal stress, which will be produced is around 10 times the shear stress. The normal stress q is a function of the square of the air gap flux density [1]:

$$q = \frac{\hat{B}^2}{2\mu_o}[\text{Pa}] \quad (1)$$

where: $\hat{B}$: air gap flux density [T or N/Am] and μ_o: permeability of free space (1.26×10^{-6} N/A^2).

Shear stress $\bar{\sigma}$ [Pa] is the most important variable in the design and is proportional to the generated torque as represented by the equation [1]:

$$T = 2\pi\bar{\sigma}R^2 l[\text{N.m}] \quad (2)$$

where: R = radius of PMG [m] and l = axial length of the PMG [m].

Shear stress $\bar{\sigma}$ [Pa] acting on the PMG is perpendicular or cut the air gap, see Figure 4. When the wave of flux density $\hat{B}$ [T or N/Am] and the electric load $\hat{K}$ is sinusoidal at an angle δ [A/m], the shear stress is [1]:

$$\bar{\sigma} = \frac{1}{2}\hat{B}\hat{K}[\text{Pa}] \quad (3)$$

B. Thermal Expansion

Besides influenced by the normal force and weight of the components, the air gap clearance is affected by dimensional changes due to heating. The heat arising from the losses occurred in the PMG causes the temperature rise and the expansion of the components. The difference in temperature rise between the stator and the rotor will cause changes in the air gap clearance, see Figure 5. Dimensional changes due to thermal expansion are calculated as [1]:

$$\Delta L = L_o \alpha \Delta T \quad (4)$$

where Δl : dimensional changes [m], α : coefficient of thermal expansion of the material [°C^{-1}], l_o: initial length [m], and ΔT: temperature rise [°C].

C. Designing Rim

Rim on the rotor serves as a retaining structure and the permanent magnet holder as demonstrated in Figure 6. In this study, it uses steel with Young's modulus of 200 GPa. Deflection on the rim, U_A is calculated using [1, 10]:

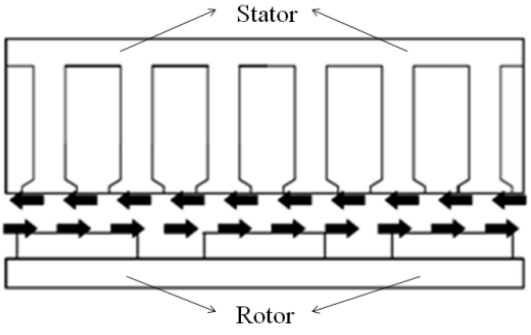

Figure 4. Cross section of the PMG with shear stress along the air gap.

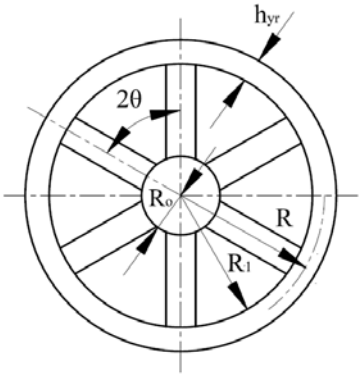

Figure 6. Cross section area of the rim.

$$U_A = \frac{qR^2}{Eh_{yr}}\left\{1 + \frac{R^3\left(\frac{k_1(sin\theta\ -\theta cos\theta\ )}{4sin^2\theta} - \frac{k_2}{2sin\theta} + \frac{k_2{}^2}{2\theta}\right)}{I\left(\left(\frac{\theta}{sin^2\theta} + \frac{1}{tan\theta}\right)\left(\frac{R}{4A} + \frac{R^3}{4I}\right) - \frac{R^3}{2I\theta}\left(\frac{1}{\left(\frac{k}{R}\right)^2 + 1}\right) + \frac{R_1 - R_o}{a}\right)}\right\} \text{[mm]} \quad (5)$$

where, R : radius of the neutral axis at the rim (143.5 mm), Ro: radius of the shaft (50 mm), Ri: radius of the rim surface (135 mm), θ: angle between the two rim (30°), A: cross-section area of the arm retaining rim (43,975 mm^2), a: cross-section area of the rim, 20,781 mm^2, I: moment of inertia rim (258,575,015 mm^4), k: radius of the rim gyration ($k = \sqrt{I/A} = 76.68\ mm$), k_1 and k_2: the correction factor of stress concentration due to momen and shear stress, and h_{yr}: thickness of the rim (10 mm).

Stress concentration at the retaining structure of the rim will result in a correction factor due to the moments and shear forces, see Figure 7. By assuming the geometry of the structure is in the form of ellipse, the correction factor can be calculated with the equation [10]:

$$k_1 = C_1 + C_2\left(\frac{2a}{D}\right) + C_3\left(\frac{2a}{D}\right)^2 \quad (6)$$

for $0.4 \le 2a/D \le 1.0$, then :

$$C_1 = 3.465 - 3.739 \times \sqrt{\frac{a}{b}} + 2.274 \times \frac{a}{b} \quad (7)$$

$$C_2 = -3.841 + 5.582 \times \sqrt{\frac{a}{b}} - 1.741 \times \frac{a}{b} \quad (8)$$

$$C_3 = 2.376 - 1.843 \times \sqrt{\frac{a}{b}} - 0.534 \times \frac{a}{b} \quad (9)$$

The correction factor due to the influence of shear force is represented by [10]:

$$k_2 = C_1 + C_2\left(\frac{2a}{D}\right) + C_3\left(\frac{2a}{D}\right)^2 + C_4\left(\frac{2a}{D}\right)^3 \quad (10)$$

for $0.5 \le a/b \le 10.0$, then:

$$C_1 = 1.000 + 2.000 \times \frac{a}{b} \quad (11)$$

$$C_2 = -0.351 - 0.021 \times \sqrt{\frac{a}{b}} - 2.483 \times \frac{a}{b} \quad (12)$$

$$C_3 = 3.621 - 5.183 \times \sqrt{\frac{a}{b}} + 4.494 \times \frac{a}{b} \quad (13)$$

$$C_4 = -2.270 + 5.204 \times \sqrt{\frac{a}{b}} - 4.011 \times \frac{a}{b} \quad (14)$$

D. Shaft Design

Shaft diameter is designed based on analytical calculations with the data inputs are weight of the components. Figure 8 shows the design of the rotor shaft construction of the PMG. The mass that must be supported by the shaft is obtained from the data of geometry and density of the permanent magnet material and rim.

Based on Figure 8, diagram of a simple free-body can be modeled to calculate the load and deflection in the shaft (see Figure 9). Force F_1 is generated from the input torque to rotate the generator while the force F_2 is generated from normal weight of the rim and the magnet. These two forces are detained by the reaction forces on the bearing R_A and R_B. To find out-loading on the shaft, the following static equilibrium equations are used [12]:

$$\left.\begin{aligned}\Sigma F &= 0\\ \Sigma M &= 0\end{aligned}\right\} \quad (15)$$

The maximum shear stress on the shaft τ [MPa] is [12]:

$$\tau = \frac{0.5\sigma_{yp}}{F_s} = \frac{16}{\pi d^3}\sqrt{((C_m M)^2 + (C_t T)^2)} \quad (16)$$

where: σ_{yp} : yield strength of the material (250 MPa for steel ST 45), F_s: safety factor, M: the maximum moment on the shaft [N.m], T: the maximum torque on the shaft from the design power [N.m], C_m: the fatigue life factor and shock loads (1.5 for initial sudden load), C_t:

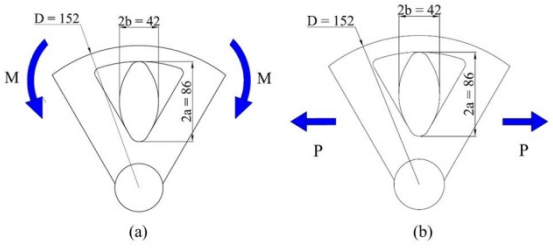

Figure 7. Correction factor due to: (a) moment and (b) shear force.

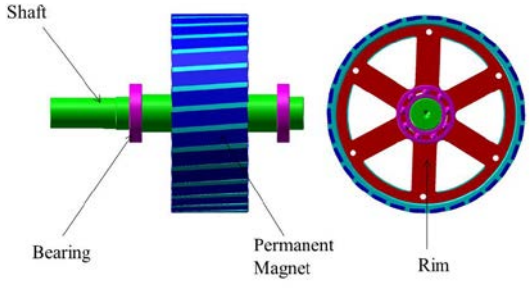

Figure 8. Rotor shaft construction.

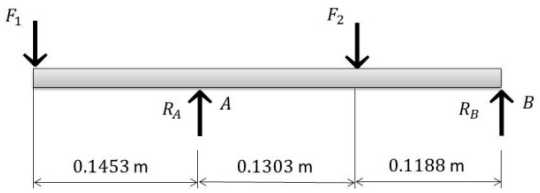

Figure 9. Free-body diagram on the shaft.

factor influenced by torque/twist (1.0 for small vibration) [11].

Based on the relationship between strain and torque curves for elastic material, shaft deflection is calculated by the equation [12]:

$$\frac{d^2v}{dx^2} = \frac{M}{EI} \tag{17}$$

where v: the elastic deflection curve [m], M: the maximum moment on the shaft [MPa], E: modulus of elasticity of the shaft material [MPa] and I: moment of inertia of the shaft [m^4].

By integrating the equation and inserting the boundary conditions on the support or bearing then the maximum deflection on the shaft can be known.

E. Finite Element Method

In general, analysis procedure using FEM consists of three steps: preprocessing, field solution, and post processing. Preprocessing comprises meshing and defining the material sand problems. In the meshing process, the continuum or area is divided into a set of finite number of elements. Defining the materials includes determination of the types of material in the sub-region, while defining the problems is the determination of the boundary conditions required as input in the calculation.

Field processing is the solution of partial differential equation based on minimizing the energy function, which is a mathematical function that relates to the potential energy stored in the system. Post processing is the extraction of the solution into a quantitative value in the form of graphs that contains all the parameters, and critical value [4].

III. Result and Discussion

A. Rim Deflection

Input data to get the rim deflection is the air gap flux density, which is calculated using the finite element solver FEMM4.2 [17]. The maximum flux density $\hat{B}$ to one pole is 1.05 T, see Figure 10.

With reference to Eq.(1), the normal stress q is 438.67 kN/m^2. Then based on Eq.(6) to (9), the constants C_1, C_2 and C_3 are 2.771, 0.582 and 1.355 respectively. The correction factor due to the moment k_1 is 2.666. From Eq.(10) to (14), the constants C_1, C_2 and C_3 each is 5.095, -5.465 and 5.406. The correction factor due to the shear stress, k_2 is 3.184. By substituting all constants and correction factors above into equation (5), 0.00452 mm of the total deflection at the rim U_A is obtained.

The result of analytical calculation of the rim deflection is further validated using FEM. Figure 11 shows the result of post processing. The maximum deflection at the rim is equal to 0.00791 mm, found at the end of the rim marked in red color. Deflection on other areas of the rim is clearly visible in accordance with subdomains or elements.

B. Shaft Deflection

Based on the geometry and material density data, the total mass that must be supported by the shaft is 29.833 kg. Multiplying the gravitational acceleration 9.8 m/s^2, thereby the load on the shaft due to the weight of the component F_2 is 292.36 N. In designing the shaft, normal stresses arising from the flux density in the air gap could be ignored because the direction is opposite to each other thus eliminating one another. From design data, the maximum power transmitted P = 10 kW and speed n = 600 rpm, as a result the maximum torque of the shaft is 159.26 N.m.

Assuming that 100 mm of a pulley diameter is mounted on the rotor then the force generated F_1 is 3,184.8 N. According to moment equilibrium law (Eq.(15)), the maximum moment acting on the shaft lies in the pedestal of the bearing A, with M = 462.75 N.m. By using Eq.(16), the maximum stress in the shaft is 62.5 MPa. Referring to the calculation results, the diameter of the shaft, which is safe from the aspect of loading with the minimum safety factor of 2 is 40 mm. However, for the ease of manufacturing, the shaft diameter is adapted to the diameter of the

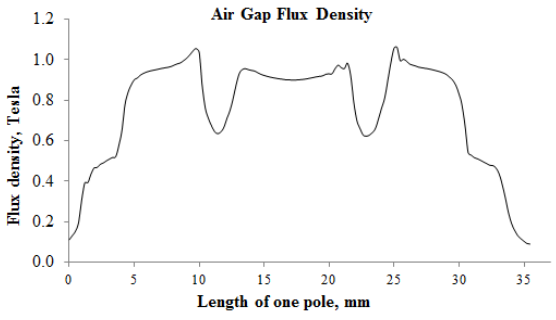

Figure 10. Flux density distributions at air gap region for one pole.

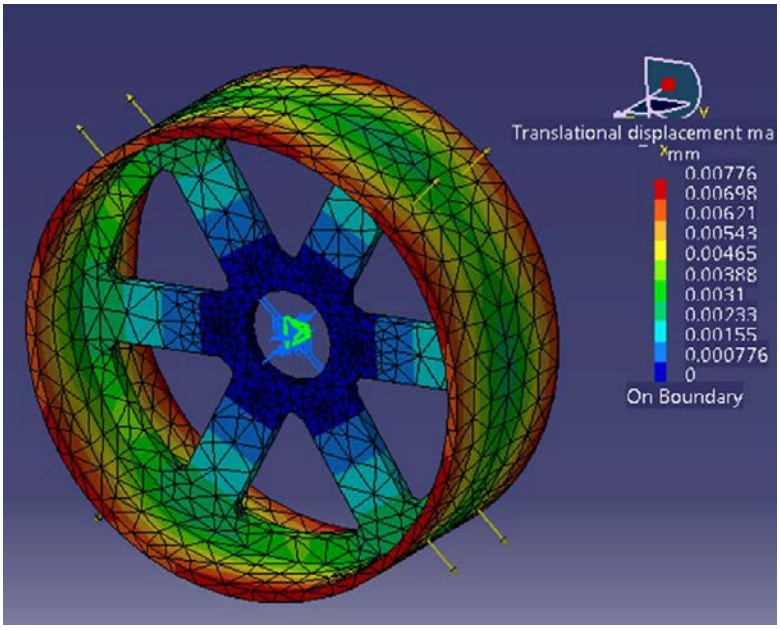

Figure 11. Deflection on the rim resulted from numerical simulation.

common bearing in the market and 55 mm of the closest diameter is determined.

By entering the boundary conditions of the bearing deflection equals to 0 then according to Eq.(17) shaft deflection is 0.0518 mm, which is found at the end part or in the area of F_1. Shaft deflection resulted from FEM simulation reaches its maximum value at 0.0246 mm or about 50% lower than the analytical calculation, see Fig.12. While the deflection at the middle or on the rim support is close to zero. Thus, 55 mm of shaft diameter is safe to use as rotor retaining structure.

C. Deflection due to thermal expansion of the material

Maximum permissible temperature of the permanent magnet (100°C) is a reference to calculate the thermal expansion of material between the stator and rotor. If the thermal expansion coefficient of steel is 2.13×10^{-6}/°C, the ambient temperature is 25°C, rotor radius R_r is 0.1680 m, and stator radius R_s is 0.1685 m, then referring to Eq.(4), the changes of rotor and stator diameters (ΔR_r and ΔR_s) are 0.166 mm and 0.167

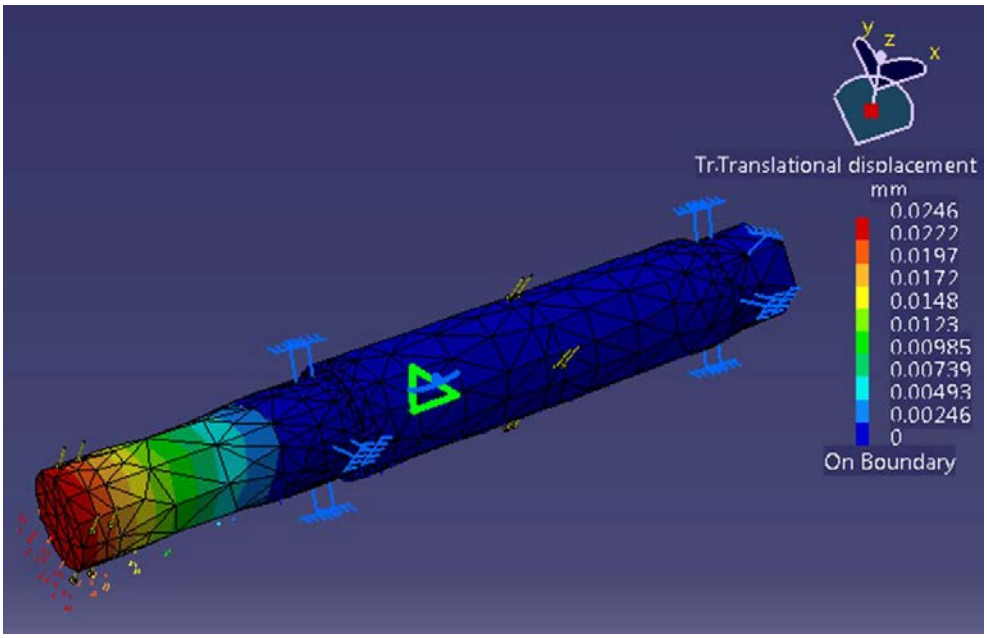

Figure 12. Shaft deflection resulted from numerical simulation.

Table 1.
Total maximum deflection on the structure of PMG.

Component	Max. Deflection (mm)	
	Analytic	Numeric
Rim	0.0045	0.0078
Shaft	0.0518	0.0246
Termal Expansion	- 0.0010 (Analytic)	
Total Deflection	0.0553	0.0314

mm respectively. Thereby the change in diameter due to thermal expansion will cause the increase of air gap opening of 0.001 mm.

D. Total Deflection on the Structure of PMG

Total deflection on the structure of PMG is the sum of the rim and shaft deflection and deflection due to thermal expansion of the material. Table 1 shows the maximum deflection for each component and the total deflection on all structures.

There is a little difference in the deflection between the analytical and simulation results; however, both are allowable because the values are still below the maximum allowable deflection (10% to 20% of the air gap clearance).

IV. CONCLUSION

- Analytical and numerical analysis of the deflection of generator structure have been discussed in this paper.
- Both analyses are each producing 0.0553 mm and 0.0314 mm of the total deflection or about 43% different. Nevertheless both are included in the safe deflection categories because the values are still below 10% to 20% of the air gap clearance.
- Based on the results, it can be concluded that 55 mm of the selected shaft rotor diameter can be safely used.

ACKNOWLEDGEMENT

The authors grateful to Directorate of Technology for Manufacturing Industry, Agency for Assessment and Application of Technology, for allowing numerical simulation using CATIA. Moreover thanks to all the team members of electric machines in The Research Center for Electrical Power and Mechatronics, Indonesian Institute of Sciences forany assistance that has been given.

REFERENCES

[1] A. S. McDonald, M. A. Mueller and H. Polinder, "Comparison of Generator Topologies for Direct-Drive Wind Turbines Including Structural Mass," *Proceedings of the International Conference on Electrical Machines (ICEM06)*, Chania, Crete, 2-5 September 2006.

[2] A. S. McDonald, M. A. Mueller and H. Polinder, "Structural Mass in Direct-Drive Permanent Magnet Electrical Generators," *Renewable Power Generation*, Vol. 2, pp. 3-15, 2008.

[3] M. A. Mueller and A. S. McDonald, "A Lightweight Low Speed Permanent Magnet Electrical Generator for Direct-Drive Wind Turbines," *Wind Energy*, Vol. 12, pp. 768-780, 2009.

[4] L. Ovacik, "Optimal Design of Nonlinier Magnetic Systems Using Finite Elements," *Journal of Engineering and Natural Sciences*, pp. 1-39, 2004.

[5] Y. Dou, Y. Gu, J. Zhu, H. Chen, and Y. Yan, "Analysis of A Hybrid Excitation Synchronous Generator Using Three Dimensional Magnetic Field Finite Element Method," *Journal of the Japan Society of Applied Electromagnetics and Mechanics*, Vol.IS, pp. S69-S72, 2007.

[6] M. S. Widyan, "Design, Optimization, Construction and Test of Rare-Earth Permanent-Magnet Electrical Machines with New Topology for Wind Energy Applications," Elektrotechnik und Informatik der Technischen Universität Berlin, Genehmigte Dissertation, 2006.

[7] M. S. Widyan and R. E. Hanitsch, "A Novel Directly Coupled High-Energy Permanent-Magnet Sinusoidal Three-Phase Generator for Wind Energy Applications," *International Conference and Exhibition on Green Energy & Sustainability for Arid Regions & Mediterranean Countries*, 2009.

[8] S.M. Hosseini, M. A. Mirsalim, and M. Mirzaei, "Design, Prototyping and Analysis of Low-Cost Disc Permanent Magnet Generator with Rectangular Flat-Shaped Magnets," *Iranian Journal of Science & Technology*, Transaction B, Engineering, Vol. 32, No. B3, pp 191-203, 2008.

[9] E. Schlemmer, "Finite Element Analysis of Electrical Machines Used in Two-Frequency Indirect Temperature Rise Tests," *International Conference on Renewable Energies and Power Quality*, 2009.

[10] A. Reinap, D. Hagstedt, F. Márquez, Y. Loayza, and M. Alaküla, "Development of A Radial Flux Machine Design Environment," *IEEE International Conference on Electrical Machines*, 2008.

[11] R.J. Roark and W.C. Young, "Roark's Formulas for Stress and Strain," 7th ed., McGraw-Hill International, 2002.
[12] Spott, M.F., "Design of Machine Elements," Prentice Hall, Tokyo, 2003.
[13] E.P. Popov, "Mechanics of Materials," 2nd Ed., Prentice Hall, USA, 1978.
[14] O.C. Zienkiewicz and R. L. Taylor, "The Finite Element Method," 5th Ed., Vol.1 The Basis, Butterworth-Heinemann, 2000.
[15] D.V. Hutton, "Fundamentals of Finite Element Analysis," McGraw−Hill Companies, 2004.
[16] S.S. Rao, "The Finite Element Method in Engineering," 4th Ed., Elsevier Science & Technology Books, 2004.
[17] D. Meeker, "Finite Element Method Magnetics," Version 4.2, User's Manual, 2009.